Bull. Inst. Chem. Res., Kyoto Univ., Vol. 65, No. 4, 1987

Superconducting Transition of $La_{1.9}Sr_{0.1}CuO_{4-\delta}$

Hiromasa MAZAKI,* Mikio TAKANO,** Zenji HIROI,** Yoshichika BANDO,**
Ryoji KANNO,*** Yasuo TAKEDA,*** and Osamu YAMAMOTO***

Received June 27, 1987

The superconducting transition of $La_{1.9}Sr_{0.1}CuO_{4-\delta}$ has been investigated in terms of complex susceptibility $\chi=\chi'-i\chi''$. The structural characterization of the specimen is made by means of the powder X-ray diffraction, the electron diffraction, and the high resolution electron microscopic observation. The susceptibility against a small ac magnetic field shows two types of response. One is insensitive to the change in the amplitude h_0 (5–1000 mOe) of the external ac field, and the other is very sensitive to h_0. In the latter case, the transition width is appreciably broadened as h_0 increases. Besides, no frequency dependence is found below 500 Hz. These behaviors are discussed with an aid of the phenomenological weak-link loop model.

KEY WORDS: La-Sr-Cu-O/ Superconducting transition/ Complex susceptibility/

I. INTRODUCTION

Since the discovery of high-T_c oxide superconductors, tremendous amount of researches has been carried out from various points of sight. Among these, the study in terms of complex susceptibility $\chi=\chi'-i\chi''$ provides a distinguishing trait. Namely, as the real part χ' and the imaginary part χ'' respectively represent different physical quantities, we can examine the superconducting nature from two different angles. As is well known, the change in χ' with respect to temperature is caused by the Meissner effect, indicating the phase transition between the superconducting and the normal state. Meanwhile, χ'' is proportional to the energy dissipation in the sample located in a periodically varying magnetic field.[1] The time-averaged variation in free energy of a material in a magnetic field is given by $Q=<-M\mathrm{d}H/\mathrm{d}t>_t$, where Q is the mean energy dissipation per unit time per unit volume, M is the magnetization, and H is a uniform external magnetic field. Substituting $h(t)=h_0\exp(i\omega t)$, one gets $Q=-(1/2)\mathrm{Re}[i\omega MH^*]=(1/2)\omega\mathrm{Im}[MH^*]$. Since χ is defined as M/H, we obtain $Q=(1/2)\omega\chi''(\omega)h_0^2$.

We prepared a series of samples with the composition of $La_{2-x}Sr_xCuo_{4-x/2+\delta}$ $(0.1\leq x<1)$ by the conventional method.[2] In this report, we present the detailed study of the complex susceptibility of one sample ($x=0.1$, 10.5 mmø, 3.4-mm thick). The observed results are discussed with an aid of the phenomenological weak-link loop model.[3]

* 間崎啓匡 : Laboratory of Nuclear Radiation, Institute for Chemical Research, Kyoto University, Kyoto 606.
** 高野幹夫, 広井善二, 坂東尚周 : Laboratory of Solid State Chemistry, Institute for Chemical Research, Kyoto University, Uji 611.
*** 菅野了次, 武田保雄, 山本 治 : Department of Chemistry, Faculty of Engineering, Mie University, Tsu 514.

II. EXPERIMENTAL

1. Sample Preparation

According to Nguyen et al.,[2] $La_{2-x}Sr_xCuO_{4-x/2+\delta}$ $(0.1 \leq x < 1)$ prepared in air at around 1373 K crystallizes in the tetragonal K_2NiF_4-type structure. In the present sample ($x=0.1$), the content of oxygen vacancies is very low (less than 1%), i.e., $\delta \simeq x/2$. The content of Cu^{3+} in the nominal composition of $La_{1.9}Sr_{0.1}CuO_4$ reaches 10%.

The sample was prepared by heating La_2O_3, $SrCO_3$, and CuO in air. An appropriate mixture of these starting materials was pressed into a pellet and was heated at 1173 K for 12 h. The product was crushed, mixed, pressed into a pellet, and fired at 1273 K for 24 h. This process was repeated twice to guarantee the compositional homogeneity. Samples with $x=0.2$ and 0.4 containing larger amounts of oxygen vacancies were also prepared and were treated under a high oxygen pressure of 2.5×10^7 Pa at 873 K to find the influences of oxygen deficiency. However, after the high pO_2 treatment, no meaningful change was observed in the measurement of superconducting transition. Henceforth, the structural characterization was made for $La_{1.9}Sr_{0.1}CuO_{4-\delta}$.

The powder X-ray diffraction (XRD), the electron diffraction (ED), and the high resolution electron microscopic observation (HRTEM) were used for structural characterization of the sample. The XRD pattern could be assigned to the tetragonal K_2NiF_4 structure with the lattice constants of $a=0.3784$ nm and $c=1.321$ nm.

The K_2NiF_4-type structure of the sample has been confirmed by observing both the ED

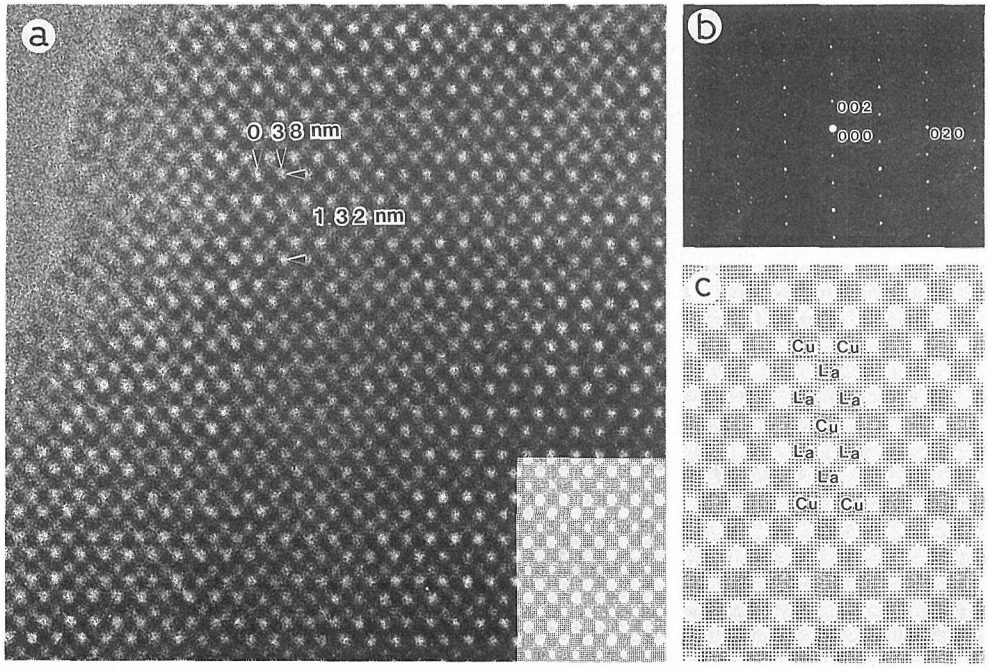

Fig. 1. (a) High resolution structure image of $La_{1.9}Sr_{0.1}CuO_{4-\delta}$ taken with an incident beam along the [100] direction. (b) Selected area diffraction pattern of the same region. (c) Simulated image revived by using the multi-slice method. The simulated image is also shown in Inset of (a).

patterns and the high resolution structure images. There have been found no ordered structures of such a small amount of oxygen vacancies. Figures 1 and 2 show images with an incident electron beam along the [100] and [110] directions, respectively. These image contrasts can be interpreted as projected charge density images; the bright dots correspond to the potential valleys surrounded by the metal atoms and the dark dots correspond to the metal atoms. In Fig 1, an ordered arrangement of double bright and single light dark dots are distinguished along the [001] direction. The former may be considered to represent the potential valleys surrounded by three La and one Cu atoms and the latter as representing those surrounded by two La and two Cu atoms. To confirm this, we made a computer simulation of image contrasts using the multi-slice method.[4] An example of the simulated images obtained is shown in Fig. 1 (c)., where we used the atomic positions determined for $La_{1.85}Sr_{0.15}CuO_4$.[5] The parameters used are a spherical aberation coefficient of 1.2 mm, a crystal thickness of 4.15 nm, an amount of defocus of 50 nm, and inclusion of 43 beams in the aperture. Fairly good agreement has been obtained between the experimental and the calculated images. Such good agreement has also been obtained for an image projected along the [110] direction as shown in Fig. 2. The bright and the light dark dots correspond to the potential valleys surrounded by four La atoms and two Cu atoms, respectively. In this way, it has been found that the high resolution structure images of $La_{1.9}Sr_{0.1}CuO_4$ can well be interpreted by assuming the K_2NiF_4 structure deduced from the XRD observation. However, it is noted that the specimen is easily damaged by the electron beam irradiation, and the structure images change their contrasts into

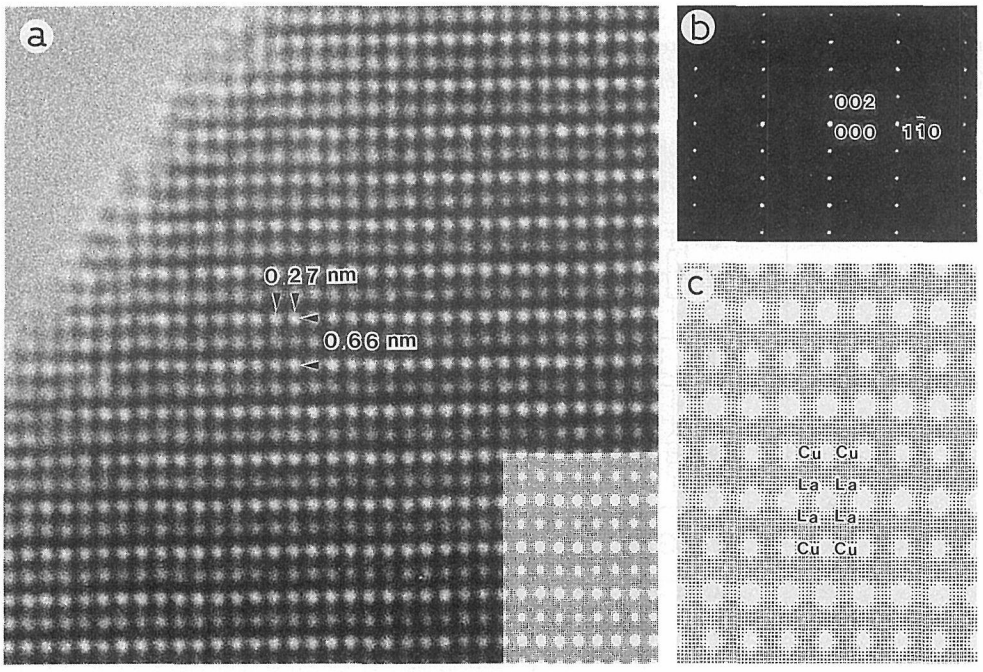

Fig. 2. (a) High resolution structure image of $La_{1.9}Sr_{0.1}CuO_{4-\delta}$ taken with an incident beam along the [110] direction. (b) Selected area diffraction pattern of the same region. (c) Simulated image revived by using the multi-slice method. The simulated image is also shown in Inset of (a).

disordered or different types. In addition, the low magnification images with an incident beam along the [001] indicate that a lot of dislocations are included in the specimen.

2. Measurements of χ' and χ''

The measuring system of the superconducting transition in terms of ac susceptibility $\chi = \chi' - i\chi''$ consists of the Hartshorn-type mutual inductance bridge[6] and the temperature control system (1.4–300 K).

The schematic diagram of the measuring system is shown in Fig. 3. The bridge has two coils, M_1 and M_2, and the phase-shift potentiometer R. The cryostat coil M_2, in which a sample is located, consists of two coaxial cylindrical coils. The ac signal into the primary circuit is fed by a function generator. The voltage signal induced in the secondary circuit of the bridge is sent to a two-phase lock-in analyzer, and then transferred to a computing digital multimeter through a universal scanner. The system is computer-controlled, and χ' and χ'' are simultaneously measured as a function of temperature. The cryostat coil was directly immersed in a liquid He bath and kept at 4.2 K. Null adjust of the bridge was made at the sample temperature of 80 K. Phase setting of the lock-in analyzer was made so as to give variation only to the in-phase signal, but not to the out-of-phase signal, against the change in the bridge inductance.

It is evident that the effect of surrounding materials to the measurement of χ should be eliminated. Paying attention to this point, a sample holder and an adiabatic cell were designed (see Fig. 4). The cell is made of pyrex glass and can be inserted in the cryostat coil. In the cell, the sample holder is hung by silk strings. At the top of the holder, we set a small Cu block, in which a calibrated carbon-glass thermometer is mounted. A sufficient thermal contact between the thermometer and the sample room is achieved through a twisted bundle of

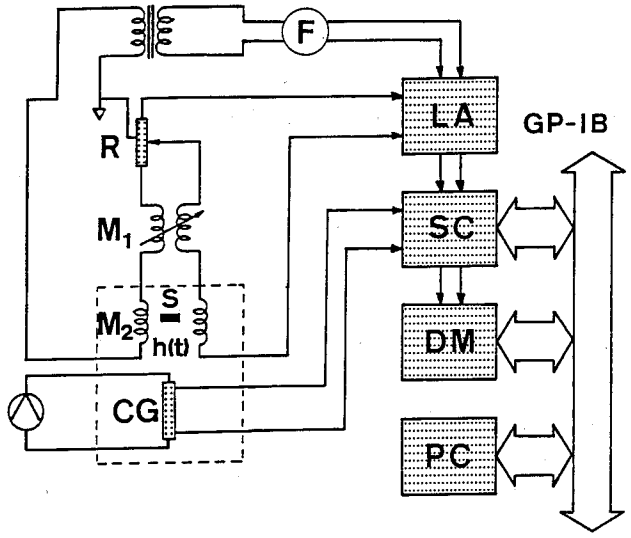

Fig. 3. Schematic diagram of the measuring system. M_1: Variable standard mutual inductance, M_2: Cryostat coil, R: Phase-shift potentiometer, S: Sample, CG: Carbon-glass thermometer, F: Function generator, LA* Two-phase lock-in analyzer, SC: Universal scanner, DM: Computing digital multimeter, PC: Personal computer.

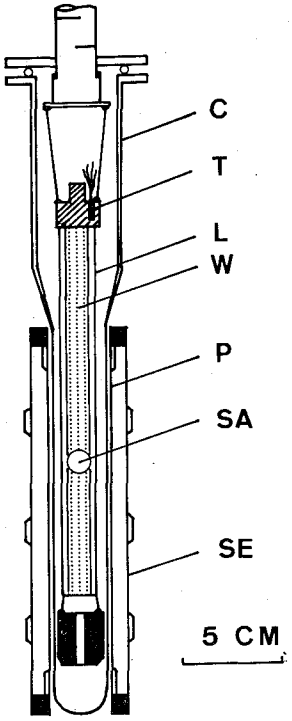

Fig. 4. Details of the sample holder and the adiabatic cell. C: Adiabatic cell, T: Carbon-glass thermometer mounted in a Cu block, L: Lucite pipe, W: Bundle of Cu wires, P: Primary coil, SA: Sample room, SE: Secondary coil.

Cu wires (0.14 mmø), and the sample is embedded in the sample room with Apieson N grease. A teflon weight used at the bottom of the sample holder is hung by silk strings. A manganin heater (0.08 mmø and 2-m long) for temperature control is wound bifilarly around the sample holder.

Since the carbon-glass thermometer is located about 10 cm apart from the specimen, one has to be very careful in the temperature control. In order to avoid the temperature gradient in the sample holder, the measurement of χ was always started at 80 K and the temperature was decreased quite slowly. Empirically, the temperature variation of 0.2 K/min guarantees the experimental error of less than ± 0.2 K.

Susceptibility measurements without a sample showed that neither the sample holder nor the adiabatic cell gives any appreciable disturbance to the measurement of χ in the temperature region to be studied.

III. RESULTS AND DISCUSSION

First, the ac susceptibility was measured under various amplitude h_0 (5–1000 mOe) of the external magnetic field $h(t)=h_0 \sin 2\pi ft$, which was applied parallel to the flat surface of the sample. Typical curves of χ' and χ'' are shown in Fig. 5, where $h_0=10$ mOe and $f=132$ Hz. In Figs. 6 and 7, we give the variation of χ' and χ'' for several different h_0 (f is fixed at 132 Hz). From Figs. 5–7, we notice the following aspects:

(a) The transition of χ' (corresponding to the Meissner effect) is quite smooth, but seems to have two phases (the lower- and higher-temperature phases).

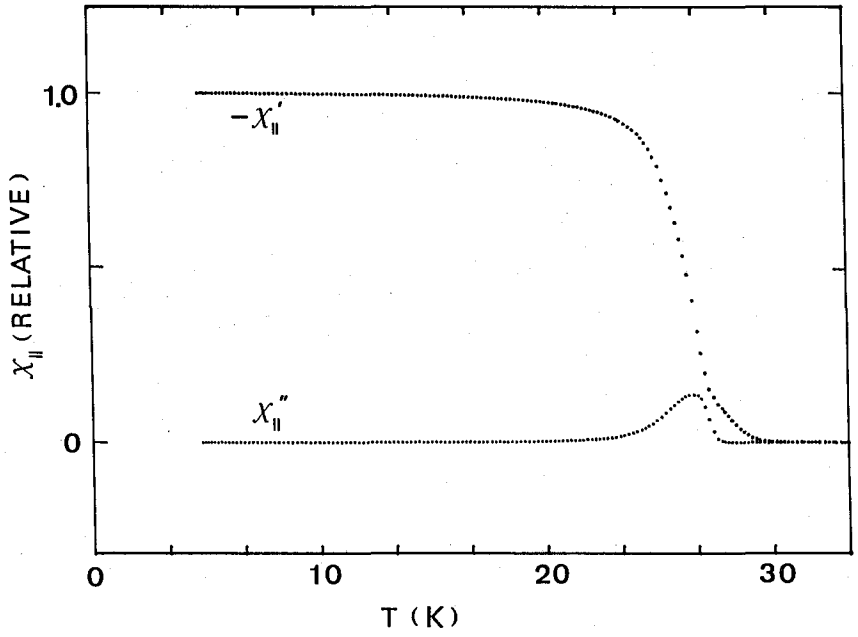

Fig. 5. Real and imaginary components of the susceptibility. The ac field is parallel to the flat surface of the disk, where $h_0=10$ mOe and $f=132$ Hz.

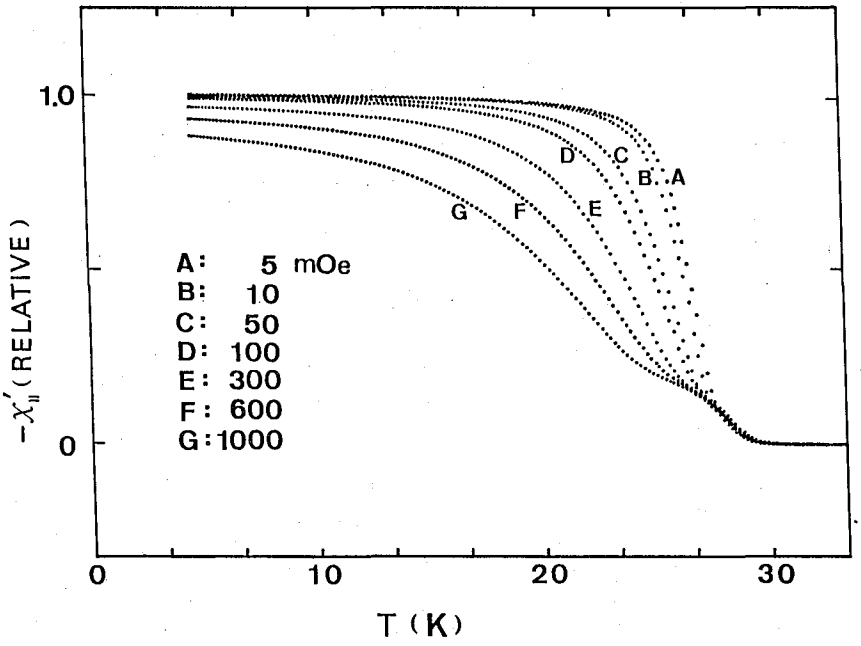

Fig. 6. h_0 dependence of the real component of the susceptibility. The ac field is parallel to the flat surface of the disk and $f=132$ Hz.

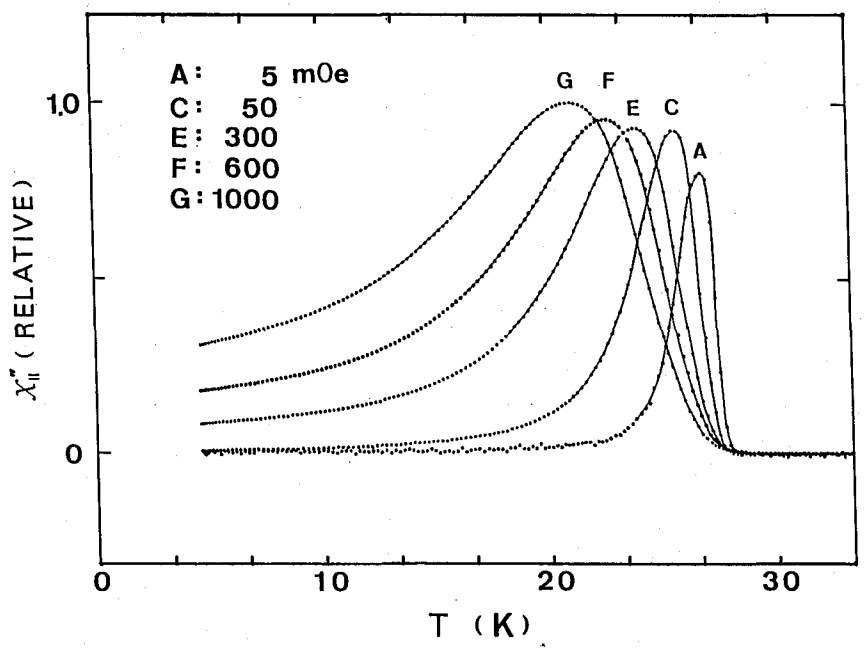

Fig. 7. h_0 dependence of the imaginary component of the susceptibility. The ac field is parallel to the flat surface of the disk and f=132 Hz. Some data are omitted for clarity.

(b) However, χ'' (being proportional to the mean energy dissipation in the sample) corresponding to the higher-temperature phase does not appear (or may be quite small), and forms a single peak in the temperature region of the lower-phase transition.

(c) For the higher-temperature phase, even χ' does not depend on h_0 in contrast with the lower-temperature phase.

(d) The transition width of the lower-temperature phase is broadened and the peak of χ'' becomes higher as h_0 increases.

(e) The onset temperatures of χ' and χ'' are almost constant.

The transition width ΔT (10–90% of χ'), the midpoint temperature T_{50} of χ', and the onset

Table I. Transition width, the midpoint of transition, and the onset temperatures for various h_0, where f=132 Hz and the ac field is parallel to the flat surface of the sample.

h_0 (mOe)	ΔT(10–90%) (K)	T_{50} (K)	χ' (ONSET) (K)	χ'' (ONSET) (K)
5	3.5	26.6	29.9	27.9
10	3.8	26.3	30.1	27.9
50	6.1	25.4	30.4	28.0
100	7.6	24.9	30.7	28.2
300	11.5	23.5	30.8	28.2
600	17.0	22.2	30.3	27.9
1000	···	20.5	30.5	28.3

temperatures of χ' and χ'' are listed in Table I. In Fig. 8, we also show ΔT and T_{50} versus h_0.

The frequency dependence of χ' and χ'' was also examined. Four different frequencies (f=80, 132, 320, 500 Hz) were used, where h_0 was fixed at 10 mOe. As shown in Fig. 9, ΔT

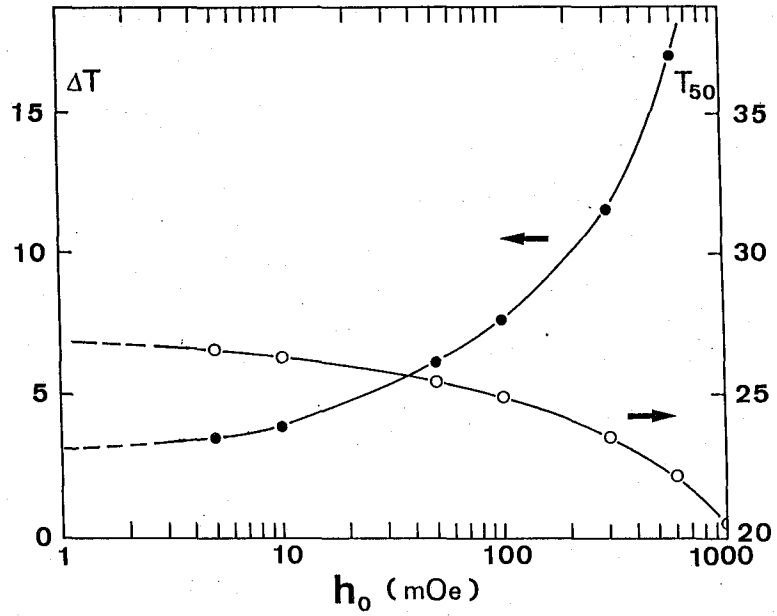

Fig. 8. Transition width ΔT(10–90%) and the midpoint temperature T_{50} versus h_0, where f=132 Hz. Both ΔT and T_{50} are in unit of Kelvin.

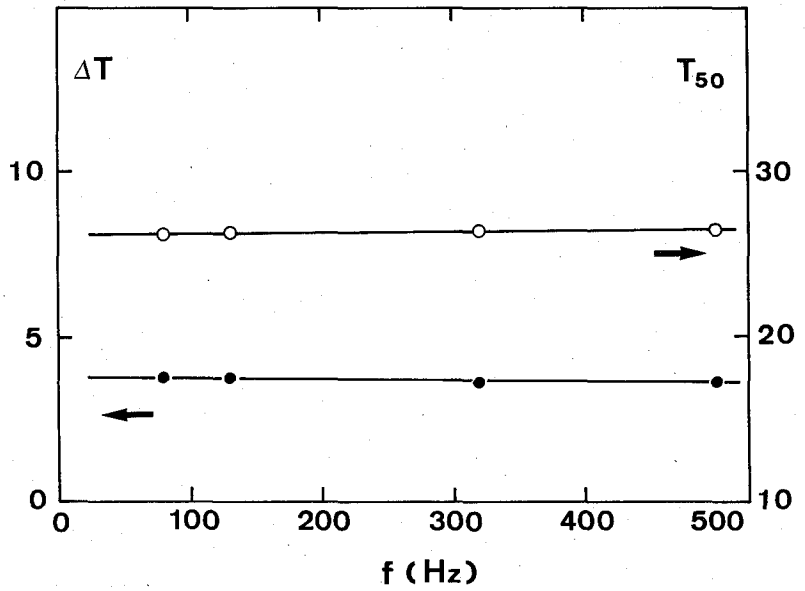

Fig. 9. Transition width ΔT(10–90%) and the midpoint temperature T_{50} versus f, where h_0=10 mOe. Both ΔT and T_{50} are in unit of Kelvin.

and T_{50} are not affected by the change in f below 500 Hz.

In order to examine the demagnetizing effect of the sample, we made similar measurements with the sample set perpendicular to the external field. Since the dimension of the disk is 10.5 mmø and 3.4-mm thick, a drastic change in the susceptibility is not expected for two different settings, parallel and perpendicular to the field. The results show that the transition curves (both χ' and χ'') are slightly broadened for the latter case, indicating the demagnetizing effect works. Typical result for χ'' is shown in Fig. 10. This discrepancy appears even for $h_0=5$ mOe and grows when h_0 is increased. However, as listed in Table II, T_{50} and the onset temperatures are the same with the parallel case.

Based on these experimental evidences, we attempt to examine the superconducting characteristics of the sample. The insensitive nature of χ' to h_0 as well as the nearly zero value of χ'' in the higher-temperature phase (28–30 K) suggest two possibilities. One is the

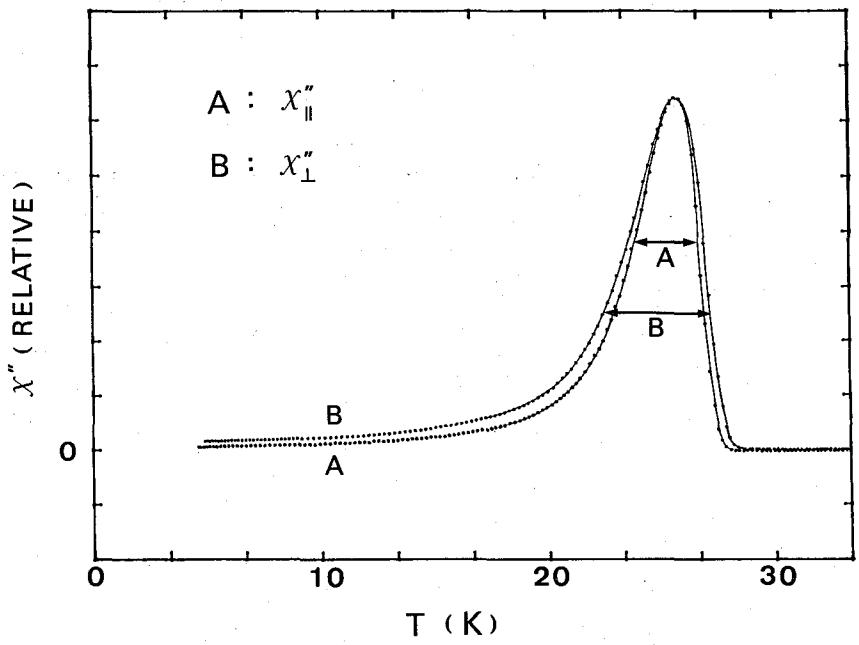

Fig. 10. Typical results of the demagnetizing effect appeared in the imaginary component of the susceptibility, where $h_0=50$ mOe and $f=132$ Hz. A and B are respectively for the ac field parallel and perpendicular to the flat surface of the disk.

Table II. Transition width, the midpoint of transition, and the onset temperatures for various h_0, where $f=132$ Hz and the ac field is perpendicular to the flat surface of the sample.

h_0 (mOe)	ΔT(10–90%) (K)	T_{50} (K)	χ' (ONSET) (K)	χ'' (ONSET) (K)
5	3.5	26.5	30.0	28.3
10	3.9	26.2	30.5	28.4
50	6.2	25.2	30.4	28.1
100	8.0	24.7	31.0	28.4

production of thin superconducting layers on the grain surface in the sample, and the layer is geometrically insensitive to $h(t)$ in terms of χ''. Note that in an ultrathin film parallel to the external field, no energy dissipation occurs.[7] Another possibility is that in that temperature region, there appear fairly solid superconducting inclusions and these regions spread over the sample volume. The negligibly small value of χ'' does not contradict to the above situation. However, we feel that the discussion below probably supports the latter case.

When the temperature is lowered further, χ'' begins to form a single peak and as seen in Figs. 6 and 7, both χ' and χ'' become very sensitive to h_0. This broadening of the transition curves is quite similar to that of a multiconnected network consisting of any kind of weak-link junctions.

Our previous work with metallic technetium embedded in a porous alumina has revealed that the ac susceptibility of the multiconnected structure can be well reproduced by the phenomenological weak-link loop model.[3] In this model, the multiconnected network behaves like a single loop as a whole due to the coherent nature of the specimen.

Assigning h_m as the magnetic field which induces the supercurrent corresponding to the Josephson critical current density $J_0(T)$ in the loop, we define $\sin\theta=h_m/h_0$. From this definition, one sees that if $h_m=h_0$ ($\theta=\pi/2$), the superconducting loop is not broken even under the maximum external field h_0 and thus the Meissner effect is completed. In other words, the superconducting transition can be expressed by this new parameter θ and the whole transition is represented by the change in θ from 0 to $\pi/2$.

In this model, χ' and χ'' are expressed in terms of θ as[3].

$$\chi'=-(1/4\pi^2)\,[\alpha-(1/2)\sin 2\alpha], \tag{1}$$

$$\chi''=-(1/4\pi^2)\sin 2\alpha \tag{2}$$

where $\alpha=2\sin^{-1}(\sin\theta)^{1/2}$. Using Eqs. (1) and (2) together with $J_0(T)$, we can draw the expected curves of χ' and χ'' versus T, where we assumed $h_0(T)$ for the Josephson tunnel junctions.[8]

In Fig. 11, we illustrate the calculated χ' and χ'' for three different external field. It is noted that the full transition from the normal state to the superconducting state is represented by $\theta=0\rightarrow\pi/2$. In the figure, one finds two features: First, when h_0 increases, the temperature T_{100} at which the transition completes, shifts to left and thus both χ' and χ'' are broadened [Compare h_0 (a) and h_0 (b)]. Second, when the frequency f is altered, any change in χ' and χ'' does not occur [Compare h_0 (a) and h_0 (c)].

The above discussion well reproduces the superconducting transition of the lower-temperature phase, the h_0 dependence of χ' and χ'' and the constancy of the onset temperatures. Besides, the insensitivity of χ to f rules out the possibility of employing the effective conducting model.[9]

However, it is evident that the behavior of χ in the higher-temperature transition cannot be explained by the above mentioned weak-link loop model. In this temperature region, certainly no weak-link structures exist.

Taking account of the whole experimental evidences found here, it seems to be plausible to think that in our sample a fairly solid superconducting phase is produced in the temperature region of 28–30 K. Then, as the temperature is lowered further, these superconducting

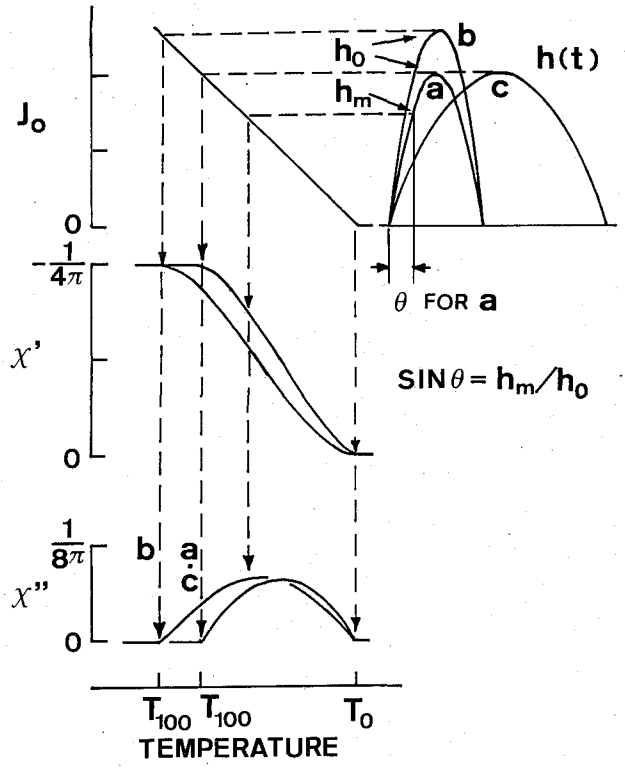

Fig. 11. Calculated χ' and χ'' for three different ac field, $h(t)=h_0 \sin 2\pi ft$. J_0 is for the Josephson tunnel junction. (a) and (b) have different h_0, but f is the same. (a) and (c) have the same h_0, but f is different. The transition is completed when $h_m=h_0$ ($\theta=\pi/2$). Note that the completion temperature T_{100} is lowered for higher h_0.

inclusions begin to couple through any kind of weak-link junctions, and form a multiconnected network.

IV. CONCLUSIONS

We measured the ac susceptibility of a $La_{1.9}Sr_{0.1}CuO_{4-\delta}$ specimen. The plausible conclusion is that in the temperature region of 28–30 K, a fairly solid superconducting phase appears. Below that temperature, both χ' and χ'' become very sensitive to the amplitude h_0 of the external ac field, and the transition width ΔT (10–90%) is broadened as h_0 increases. The peak height of χ'' is also h_0 dependent and is enhanced when h_0 is increased. However, the onset temperatures of χ' and χ'' stay constant for all h_0 measured. It has been also revealed that both χ' and χ'' are insensitive to the frequency of ac field below 500 Hz. These fundamental behaviors can be qualitatively understood by the phenomenological weak-link loop model. The smallness of the critical current density of this kind of materials may come from this weak-link characteristics.

Our recent works with 90-K class superconductors, $ErBa_2Cu_3O_{6+x}$[10] and $YBa_2Cu_3O_x$,[11] have revealed that the characteristics are essentially the same with the present case. This

strongly suggests that the features presented here are probably common for high-T_c oxide superconductors produced by the sintering process.

ACKNOWLEDGMENTS

Disscussion with Dr. T. Ishida and Dr. K. Kanoda is acknowledged.

REFERENCES

(1) L. D. Landau and E. M. Lifshitz, "Electrodynamics of Continuous Media", Addison-Wesley Publishing Company, Inc., Reading, Massachusetts, (1960), Chap. 7.
(2) N. Nguyen, J. Choisnet, M. Hervieu, and B. Raveau, *J. Solid State Chem.*, **39**, 120 (1981).
(3) T. Ishida and H. Mazaki, *J. Appl. Phys.*, **52**, 6798 (1981).
(4) P. Goodman and A. F. Moodie, *Acte Cryst.*, **A30**, 280 (1974).
(5) R. J. Cava, A. Santoro, D. W. Johnson, Jr., and W. W. Rhodes, *Phys. Rev. B*, **35**, 6716 (1987).
(6) L. Hartshorn, *J. Sci. Instr.*, **2**, 145 (1925).
(7) K. Kanoda, H. Mazaki, N. Hosoito, and T. Shinjo, *Phys. Rev. B*, **35**, 8413 (1987).
(8) V. Ambegaokar and A. Baratoff, *Phys. Rev. Lett.*, **10**, 486 (1963).
(9) E. Maxwell and M. Strongin, *Phys. Rev. Lett.*, **10**, 212 (1963).
(10) T. Ishida and H. Mazaki, *Jpn. J. Appl. Phys.*, **26**, L1296, L1508 (1987).
(11) H. Mazaki, M. Takano, Y. Ikeda, Y. Bando, R. Kanno, Y. Takeda, and O. Yamamoto, *Jpn. J. Appl. Phys.*, **26**, L1749 (1987).